CHPATER　4

THERMAL STABILITIES OF OHMIC CONTACT

AND SCHOTTKY CONTACTS TO GAN

4.1 Electrical Contact to GaN

GaN is attractive for optical devices emitting at blue or ultraviolet wavelengths as well as for high power and high temperature electronics. Critical to the success of these devices, however, are the Ohmic contacts, and in some cases Schottky contacts to the semiconductors. In general, making low-resistance Ohmic contact is difficult for wide bandgap materials, especially for p-type GaN due to the difficulty in doping. This creates a large voltage drop across the GaN/metal interface for Ohmic contacts, which leads to poor device performance and reliability. For most devices, Ohmic contacts with resistances lower than $10^{-5}\Omega cm^2$ is desired.

Ti-based contacts with contact resistance of 10^{-6}-$10^{-5}\Omega cm^2$ have been demonstrated on n-type GaN [1-3]. Thes contacts take advantage of the formation of a thin interfacial TiN layer, which is refractory, exhibiting metallic conductivity, and possess low work function (<4eV) [4]. However, no satisfying Ohmic contact to p-type GaN hase been developed so far. In the search for improved contact characteristics, a wide variety of metallizations have been investigated on p-GaN besides the standard Ni/Au [3,5-7], including Ni [8-9], Pd [8], Pd/Au [10], Pt/Au [11], Au/Mg/Au [12], and Pd/Pt/Au [11]. Typically metals with large work function such as Ni, Pd pr Pt are in direct contact with the GaN, and the structure is annealed at 400-750℃. This produces contact resistances in the 10^{-1}-$10^{-3}\Omega cm^2$ range. Reports have also appeared on the effect of annealing in O_2 ambient in reducing r_c [13],

oxidation of Ni/Au metallization and its role in improving contact quality [14], the role of surface treatments in determining contact quality [15-16] and the use of Ta/Ti contacts with low, but unstable contact resistances [17]. Another approach to achieve low-resistance contact is through semiconductor bandgap engineering. Schubert *et al.* [18] proposed the use of AlGaN/GaN superlattices as a technique to increase the average hole concentration. The periodic oscillation of the valence band edge is superimposed with the oscillation generated by piezoelectric field, would significantly reduce the Mg acceptor ionization energy, and therefore, increase the hole concentration. Ti/Pt/Au contacts with specific contact resistance of $\sim 4 \times 10^{-4} \Omega cm^2$ have been achieved on this structure [19]. However, this scheme may not easily be applied to real devices, since the free carriers were separated into parallel sheets.

The Schottky contacts to n-GaN for a variety of elemental metals have been extensively studied. The reported Schottky barrier heights increase monotonically, but do not scale proportionally with the metal work function, with a considerable amount of scatter in the experimental results for a given metal. The *I-V* ideality factor is usually significantly larger than 1, and the measured values of the Richardson's constant A^{**} are quite small [20]. These non-ideal behaviors of GaN Schottky diodes appear to result from the presence of several transport mechanism, and to materials and process factors such as defects present in these films, the effectiveness of surface cleaning prior to metal deposition, local stoichiometry variations, and variations in the surface roughness, as discussed in previous chapter.

One of the important issues in making high quality Schottky and Ohmic contacts to GaN is the surface cleanliness [21]. The ideal metal/semiconductor interface should be oxide- and defect-free, atomically smooth, uniform, and thermally stable, with the metal being epitaxial. Analysis by spectroscopic ellipsometry showed that more than 30Å of the overlayer consists of organic and inorganic, and native oxide is present on

the air-exposed GaN [10]. In situ treatments, such as N ion sputtering, were reported to remove oxide layer on the GaN surface without significant modification of the N to Ga atomic ratio [7,22]. For practical contacts, the samples were treated with various acidic or base solutions before deposition of the metal layers. It was found that HCl-based solution is more effective in removing oxides and leaves less oxygen residue, but HF is more effective in removing carbon and hydrocarbon contaminations [23].

The thermal stability of metal/GaN contacts is also of initial importance for practical device operation (especially power electronics). The thermal stability limits of most of the metal/GaN combinations are between 300℃ and 600℃ [20]. At higher temperatures, severe degradation in contact morphology is observed, usually resulting from the formation of new interfacial phases, such as metal gallides.

In order to realize the materials for high temperature applications, high quality Ohmic and Schottky contacts operating under high temperature without deteriorating the performance of the devices is required. The Schottky barrier heights of a variety of elemental metals including Ni, Au, Pt, and Pd on n-GaN have been investigated [24]. The thermally stable Schottky materials such as Ni, NiSi, Pt, PtSi, Pd, Re, PdIn, and Ni/Ga/Ni have also been reported [25-28]. Some studies on Ni and Pt silicides also show that silicides are ideal candidates as thermal stable contacts for GaN due to the inertness of the interface between the silicide layer and the GaN substrate [25-26].

The refractory metal nitrides exhibit excellent thermal stability and form stable Schottky contact with GaAs after high temperature annealing by the self-aligned gate technology [29-30]. TiWN$_x$/Ga$_{0.51}$In$_{0.49}$P contact with excellent thermal stability and electrical characteristics has also been demonstrated with barrier height and ideality factor of 1.00 eV and 1.04, respectively, after rapid thermal annealing (RTA) at 850℃ for 10 seconds [31]. However, the Schottky contact characteristics of the refractory

transition metal nitrides such as titanium tungsten nitride ($TiWN_x$) and tungsten nitride (WN_x) with GaN have never been investigated.

In the thesis, the thermal stability of Ti/Al/Ni/Au and Ti/Al/Pt/Au Ohmic contacts were verified at different temperatures. As to the Schottky contacts, the $TiWN_x$ and the WN_x films were deposited by reactive dc sputtering method, both the electrical characteristics and material aspects of the GaN Schottky contacts were investigated. The electrical properties were characterized by current-voltage measurement and the material properties were characterized by low angle X-ray diffraction, secondary ion mass spectroscopy (SIMS) methods.

4.2 Experimental

4.2-1 Starting Materials

In this study, two different epitaxial layers of n-GaN samples and one n-Al_XGa_{1-X}N sample with 0.06 aluminum mole fraction were grown on (0001) sapphire substrates by metal-organic vapor phase deposition method (MOCVD). GaN with carrier concentration 4.4×10^{18} cm^{-3} were used in the study of Ohmic contact, while GaN with carrier concentration 1.8×10^{17} cm^{-3} was used in the study of Schottky contact. The layer structures are illustrated in Figures 4-1(a), (b) and (c), respectively. The results of Hall measurement at room temperature are shown as Table IV.

4.2-2 Surface Cleaning

Prior to the Ohmic and Schottky contact fabrication, removal of native oxides, organic contaminants, metallic impurities and residual species from the epilayer were

carried out. The cleaning steps are listed as follows:

(a) Soak in acetone with ultrasonic agitation for 5 min;

(b) Rinse in D.I. water for 5 min;

(c) Dry by N_2 gas;

(d) Dip into the solution of HCl : H_2O = 1 : 1 for 5 min;

(e) Rinse in D.I. water for 5 min;

(f) Dry by N_2 gas;

(g) Dip into BOE for 3 min;

(h) Rinse in D.I. water for 5 min;

(i) Dry by N_2 gas.

4.3 Ti/Al/Ni/Au and Ti/Al/Pt/Au Ohmic Contacts to GaN

The multilayer metals Ti/Al/Ni/Au (200Å/2000Å/500Å/600Å) and Ti/Al/Pt/Au (400Å/800Å/1400Å/1500Å) were deposited using an electron-beam evaporating system on n-GaN and n-AlGaN respectively for the study of Ohmic contact. The deposition rate of the metals was about 5Å/sec. We prepared a rectangular contact pads on GaN by depositing Ti/Al/Ni/Au (200Å/2000Å/500Å/600Å) through a metallic mask and carried out RTA annealing at 900℃, 30 sec in N_2 gas to form the Ohmic contact.

In order to lower the specific contact resistance of the Ohmic contacts, thermal annealing for metal alloying is necessary. The metals Ti/Al/Ni/Au with thickness 200Å/2000Å/500Å/600Å were deposited on n-GaN and n-AlGaN; Ti/Al/Pt/Au (400Å/800Å/1400Å/1500Å) were deposited on n-AlGaN, these metals were annealed by a RTA system to form low-resistance Ohmic contact. The samples with Ti/Al/Ni/Au were annealed in the temperatures range from 500℃ to 900℃ for 30 seconds with each increment step of 100℃, while samples with Ti/Al/Pt/Au were

annealed at 950℃ for 35 sec, 60 sec and 120 sec. All the annealing processes were in a N$_2$ atmosphere.

The circular test structure of CTLM has one main advantage: the contact design avoids the need to isolate the metallization structures by etching. In this work, the outer contact radius R_1 equals 200 μm and the circular electrodes have the spacing of 5, 10, 15, 25, 35, and 45 μm respectively as shown in Fig. 4-2(a).

The specific contact resistivity ρ_c, is determined using the method of CTLM [32]; the total resistance R_T is plotted against gap spacing d, as shown in Fig. 4-2(b), the contact resistance R_C and the transfer length L_T are extracted by y- and x- axis intercept respectively. The sheet resistance ρ_s can be determined from the following equation:

$$R_T = \frac{\rho_s}{2\pi} \cdot [\ln(\frac{R_1}{R_1 - d}) + L_T \cdot (\frac{1}{R_1 - d} + \frac{1}{R_1})] \qquad (4\text{-}1)$$

For $2\pi R_1 \gg d$, the equation above can be simplified according to the standard TLM structure [33] which provides a linear relationship as:

$$R_T = \frac{\rho_s}{2\pi R_1}(d + 2L_T) \qquad (4\text{-}2)$$

Finally, the specific contact resistivity can be determined by:

$$\rho_C = \rho_s \cdot L_T^2 \qquad (4\text{-}3)$$

For practical ring radii (200 μm) and gaps (5 – 45 μm), small correction factors are necessary to compensate the difference of TLM and the ring layouts to get a linear fit to the data. The calculated correction factors are given in Figure 7(a) for a constant outer radius of 200 μm and a varying gap distance. Without these correction factors, the specific contact resistivity will be underestimated.

The *I-V* characteristics for Ti/Al/Ni/Au Ohmic metal with n-GaN after annealing

are shown in Fig. 4-3. The annealing temperature is from 500℃ ~ 900℃ with increment step of 100℃, the annealing time is 30 sec and the annealing is performed using RTA in N_2 ambient. The Ohmic metal gap in this measurement is 10 μm. The I-V curves exhibit non-linear behavior for those annealed at 500℃ and 600℃. The results revealed that they were not Ohmic contacts. The I-V curve become linear after annealed at higher temperatures (700℃~900℃). The specific contact resistivities of the Ohmic contact were calculated by the reciprocal of the differential at a voltage of 0.5 V. According to section 4.2-5, the total resistance (R_T) is plotted against gap spacing, as shown in Fig. 4-4. The specific contact resistivity ρ_c, contact resistance R_c, sheet resistance ρ_s and transfer length L_T of n-GaN after RTA treatment were extracted and listed in Table V, while the specific contact resistivity as a function of annealing temperature is shown in Figure 4-5. The specific contact resistivies ρ_c were determined to be 7.16×10^{-5} Ω·cm², 4.00×10^{-5} Ω·cm² and 3.46×10^{-6} Ω·cm² ; the values of contact resistance were 0.54 Ω·mm, 0.49 Ω·mm and 0.16 Ω·mm; results of transfer length were extracted to be 9.74 μm, 9.34 μm and 1.70 μm; while the sheet resistance were 75.50 Ω/□, 45.85 Ω/□ and 119.72 Ω/□. The data were taken after 700 ℃, 800℃ and 900℃ annealing respectively. According to Table V, the specific contact resistivity ρ_c decreased as the annealing temperature increased. Also, the annealing at 900℃ resulted in the lowest value of specific contact resistivity, contact resistance and transfer length, as revealed in Table VI.

Figure 4-6 shows the I-V characteristics of the Ti/Al/Ni/Au multilayer contacted on n-AlGaN with the equal gap of 10 μm. After 700℃, 800℃ and 900℃ annealing in N_2 ambient for 30 sec the contacts showed the linear I-V characteristics, this means that the Ohmic behavior occurred after the annealing processes. The plots of resistance against gap spacing are illustrated in Fig. 4-7. The values of specific contact resistivity ρ_c, contact resistance R_c, sheet resistance ρ_s and transfer length L_T

are also determined by x-, y-axis intercept using equation (4-2) and the results are summarized in Table VI. The optimum annealing temperature for n-AlGaN is 700℃, the specific contact resistivity, contact resistance, transfer length and sheet resistance were 2.09×10^{-6} Ω·cm², 0.23 Ω·mm, 1.95 μm and 152 Ω/□ respectively. The plot of specific contact resistivity as a function of annealing temperature is shown in Fig. 4-8. The specific contact resistivity decreased when the temperature was raised to 800℃ and 900℃.

Figure 4-9 showed the I-V characteristics of the Ti/Al/Pt/Au multilayer contacted on n-AlGaN with equal gap of 10 μm. The entire curve exhibits a linear characteristic, including the as-deposited sample. The results listed in Table VII were extracted from Fig. 4-10, which is plotted by total resistance against gap spacing. Figure 4-11 shows the variation of ρ_c *versus* annealing time. As the annealing time increases, the ρ_c becomes lower, the best value of ρ_c was 7.50×10^{-6} Ω·cm² after annealing at 950℃ for 60 sec in N_2. The value of ρ_c degraded when annealing time increases to 120 sec.

Optimum annealing conditions to form low contact- resistance Ohmic contact were achieved in this study. The best result of specific contact resistivity ρ_c corresponds to an optimum annealing condition for different materials are listed in Table VIII. GaN with Ti/Al/Ni/Au as the Ohmic contact has the lowest specific contact resistivity after annealed at 900 ℃ for 30 sec in N_2, while Ti/Al/Ni/Au/n-AlGaN contact has the lowest specific contact resistivity after annealed at 700℃ for 30 sec in N_2. Our experimental results indicated the Ti/Al/Ni/Au multilayer metal forming superior Ohmic contact for n-type GaN and n-type AlGaN.

However, except for low resistivity, long-term thermal stability is also important for the device applications. In Ti/Al/Ni/Au system, Ni plays a role to prevent the diffusion of Au (oxidation cap) into Ti/Al bilayer [34-35]. Pt has been approved to be a good diffusion barrier as Ni does [36]. C. T. Lee *et. al.* demonstrated that

Ti/Al/Pt/Au Ohmic contact to n-GaN possessed a long-term thermal stability up to 600 minutes [37]. That's why we chose Ti/Al/Pl/Au as Ohmic contact for our HEMT device.

4.4 TiWN and WN Schottky Contacts to GaN

The titanium tungsten nitride and tungsten nitride were deposited by dc-magnetron reactive sputtering of Ti/W (1/10 atomic ratio) target and pure W (99.99%) target in an Ar and N_2 mixture onto GaN. Prior to sputtering, the deposition chamber was pumped down to 1.6×10^{-6} Torrs, and then pre-sputtered for 20 min in a mixture of Ar and N_2 gases. The flow rate of the Ar gas was 24 sccm, and the N_2 gas was 4.8 sccm; deposition rate of these films were 30 Å/min and 24 Å/min, respectively. The sputtering was performed at 200 W of dc power with a total pressure of 7.6×10^{-3} Torr. The final thickness of these films was about 2000 Å. The diameter of the Schottky pattern was 1 mm.

An HP-4145B semiconductor parameter analyzer was used to measure the I-V characteristics of the Schottky diodes. At room temperature (300K), according to the thermionic emission theory, thermal emission dominates the carriers conduction mechanism of the Schottky diodes, the forward I-V characteristics of the diode can be described by the equation:

$$I = I_0 \left[\exp\left(\frac{qV}{nkT} \right) - 1 \right]$$
(4-4)

and

$$I_0 = AA^{**}T^2 \left[\exp\left(\frac{-q\phi_b}{kT} \right) \right]$$
(4-5)

In this measurement, we took the part of forward bias which applied to the diodes and the equations above can be rewritten as:

$$I = I_0 \exp\left(\frac{qV}{nkT}\right)\left[1 - \exp\left(\frac{-qV}{kT}\right)\right] \quad\quad (4\text{-}6)$$

According to the equation (4-6), the ideality factor n can be extracted from the slope of the plot of $ln[I/(1\text{-}exp(\text{-}qV/kT))]$ versus V. Schottky barrier height ψ_b, could also be extracted by the y-axis intercept. The values of $\boldsymbol{n}$ and ψ_b can be calculated by:

$$n = \left(\frac{kT}{q} \cdot slope\right)^{-1} \quad\quad (4\text{-}7)$$

and

$$\phi_b = \frac{kT}{q} \cdot \left[In\left(AA^{**}T^2\right) - \left(y - \text{intercept}\right)\right] \quad\quad (4\text{-}8)$$

where $\boldsymbol{k}$ is Boltzmann constant, $\boldsymbol{T}$ is the absolute temperature, and $\boldsymbol{A^{**}}$ is the effective Richardson coefficient.
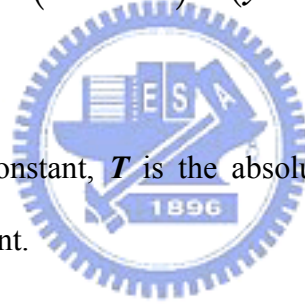
4.4-1 DC Characteristics of the TiWNx and the WN Schottky Contacts to GaN

The logarithmic plot of current against applied voltage for $TiWN_x$ and WN_x/GaN Schottky diodes are shown in Fig. 4-12 and Fig. 4-13. Figure 4-12 showed that the leakage current density of the as-deposited $TiWN_x$ diode was about 3×10^{-5} A/cm^2 at 1 V, dropped an order of magnitude after annealing at 650℃, and increased an order of magnitude after annealing at 750℃. It changes to Ohmic-like behavior when annealed at 850℃. The leakage current densities of WN_x Schottky diodes remained at the order of 10^{-7} A/cm^2 after annealing at all temperatures as shown in Fig. 4-13.

Obviously, TiWN$_x$ film was only thermally stable up to 650℃, while WN$_x$ Schottky contact remained stable and show only slight change on leakage current density after annealing at temperature as high as 850℃.

According to section Eqn. 4-7 and Eqn. 4-8, the ideality factor and Schottky barrier height were determined from the slope and *y*-intercept of the curve in the range from 0.1 to 0.4V. Figure 4-14 and Fig. 4-15 show the results extracted for TiWN$_x$/GaN and WN$_x$/GaN respectively. The calculated ideality factor and Schottky barrier height are summarized in Tables IX. The barrier height and ideality factor for as-deposited TiWN$_x$/GaN were 0.71 eV and 1.17, respectively. After annealing at 650 ℃, the diode characteristics were improved with the barrier height of 0.76 eV and an ideality factor of 1.14. At T_A = 750℃, the barrier height and the ideality factor degraded to 0.65 eV and 1.19, respectively. The Schottky contact changed to an Ohmic-like behavior after 850℃ annealing.

The barrier height and ideality factor of the as-deposited WN$_x$/GaN are 0.67 eV and 1.15, respectively. The diodes behavior improved with the increase of annealing temperature. After annealing at 650℃, the barrier height and the ideality factor improved to 0.83 eV and 1.10. At T_A = 750℃, the barrier height and ideality factor were 0.80 eV and 1.10, respectively. A barrier height of 0.80 eV and an ideality factor of 1.09 were observed when the annealing temperature was raised to 850℃.

The Schottky diode characteristics improvements after 650℃ annealing were attributed to the removal of the sputter-induced damages between the metal/GaN interfaces during thermal annealing process. However, WN$_x$ diode was thermally stable up to 850℃, while TiWN$_x$ diode was only stable up to 650℃. In conclusion, the WN$_x$ film as a Schottky contact on n-type GaN was more stable than TiWN$_x$ as a Schottky contact to n-GaN after thermal annealing at elevated temperatures.

Figure 4-16 and Fig. 4-17 showed the leakage currents of TiWN$_x$ and WN$_x$ diodes.

We found that the diode with highest breakdown voltage was the diode with the highest Schottky barrier height. This is in agreement with the theoretical prediction.

4.4-2 Material Characterizations of TiWNx and WN Schottky Contacts to GaN

The phases of the $TiWN_x$ and WN_x films before and after thermal annealing were characterized by low angle X-ray diffraction. The X-ray spectra of the $TiWN_x$ and WN_x films as a function of annealing temperature are shown in Fig. 4-18 and Fig. 4-19 respectively. Because the x-ray beam has a small incident angle of 0.8^o, the substrate GaN (0002) peak wasn't observed in the diffraction pattern.

As can be seen from the X-ray diffraction patterns in Fig. 4-18, the phase formed in the WN_x film was identified as β-W_2N phase. Figure 4-19 shows the lattice parameters of the WN_x and the $TiWN_x$ films before and after annealing. The lattice parameter of the as-deposited WN_x film is higher than the corresponding bulk value of the W_2N phase which is 4.126 Å. This is attributed to the expansion of the lattice constant by the incorporation of excessive nitrogen atoms, because the lattice parameter increases with increasing nitrogen composition x in the WN_x phase [38]. In the case of over-stoichiometric N/W ratio in the film, the excessive nitrogen atoms could occupy the vacant octahedral sites, resulting in an expansion of the W_2N lattice [39]. A continuous shift of the diffraction peaks toward higher 2θ is observed. The lattice parameter of the WN_x film decrease from 4.158 Å to 4.135 Å after annealing at 650°C. This was due to the out diffusion of the excess nitrogen atoms from the WN_x film during high temperature annealing treatment, resulting in a reduction of the lattice parameter. After annealing at 850°C, the lattice parameter value approached to 4.126 Å which is the reported bulk value of W_2N phase.

From the X-ray diffraction results in Fig. 4-19, the $TiWN_x$ films formed TiW_2N

phase with dissolved Ti after DC sputtering deposition. Judged from the X-ray analysis data for the peak in the reference [40], the phase is a solid solution with Ti in W_2N. The as-deposited WN_x and $TiWN_x$ film has a preferred (220) and (111) texture respectively after sputtering deposition. The intensity of the peaks of the preferred (220) texture of the $TiWN_x$ film increased with increasing annealing temperature. When compared to the as-deposited W_2N phase, the TiW_2N solid solution phase has a larger lattice parameter due to the dissolved titanium atoms in the $TiWN_x$ film as shown in Fig 4-20. The lattice parameter of the $TiWN_x$ film decreased from 4.172Å to 4.162Å when annealing temperature was increased from 650℃ to 850℃, this was possibly due to the out diffusion of the nitrogen atoms from the $TiWN_x$ film and the diffusion of the Ti and W atoms into the GaN substrate after annealing at higher temperatures.

To verify what has occurred at the refractory metal nitrides/n-GaN interface, both $TiWN_x$/n-GaN and WN_x/n-GaN samples were subjected to secondary ion mass spectroscopy (SIMS) depth profiling analysis before and after thermal treatment up to 850℃. A smooth sample surface is important in order to obtain good SIMS depth resolution. If the sample surface is not smooth, the surface irregularities will replicate into underlayers and reduced the depth resolution of a sharp interface. Figure 4-21 shows the surface profile of WN_x and $TiWN_x$ film before and after annealing at 850℃. From the AFM results, the surface roughness doesn't give an influence on the interface analysis with SIMS depth analysis. Figure 4-22(a)~(c) are the SIMS depth profiles of the $TiWN_x$/n-GaN interface as deposited and after annealed at 650℃ and 850℃, as can be see from Fig. 4-22(a), the $TiWN_x$/n-GaN interface remained sharp after 650℃ annealing, however, the atomic inter-diffusion between $TiWN_x$ and GaN materials occurred after 850℃ annealing as shown in Fig. 4-22(c). This is in agreement with the electrical data shown in Table V which shows that the barrier

height of the WN_x/n-GaN diode dropped to 0.62eV and the ideality increased to 1.54 after 850℃ annealing. For the WN_x/n-GaN contacts, there's no detectable inter-diffusion between WN_x and n-GaN after 650℃ and 850℃ annealing as can be seen from the SIMS data shown in Fig. 4-23(b) and Fig. 4-23(c). The result is in agreement with the data observed in Table IV. From the electrical characteristics of the WN_x/n-GaN Schottky shown in Table IV, the Schottky contact remained quite stable after 850℃ annealing with the barrier height remained at 0.80 eV and the ideality factor remained at 1.09. The electrical characteristics and the materials analysis showed that the WN_x/n-GaN interface was metallurgically stable up to 850℃.

In conclusion, the electrical characteristics and the materials aspects of the refractory $TiWN_x$ and WN_x films as the Schottky contacts on n-type GaN were studied. From the low angle X-ray diffraction data, the WN_x film formed β-W_2N phase and the $TiWN_x$ film formed TiW_2N solid solution with Ti atoms dissolved in the β-W_2N lattice after deposition. Lattice parameter measurement on the WN_x films indicated a β-W_2N unit cell with lattice parameter larger than the reported data, which is due to the incorporation of excessive nitrogen atoms in the β-W_2N lattice. The lattice parameter of the β-W_2N phase and the TiW_2N solid solution decreased with increasing annealing temperature, which is believed to be due to the out diffusion of the N atom from the β-W_2N and the TiW_2N lattices. The WN_x Schottky contact to n-GaN was thermally stable up to 850℃, and the ideality factor and the barrier height remained at 1.10 and 0.80 eV, respectively after 850℃ annealing. The Schottky characteristics of the $TiWN_x$/n-GaN contact remained stable up to 650℃ annealing with the ideality factor and the barrier height remained at 1.14 and 0.76 eV, respectively. The contact degraded after 750℃ annealing and become Ohmic-like behavior after 850℃ annealing. This degradation of the diode was due to the atomic

inter-diffusion between $TiWN_x$ and GaN which occurred at higher temperatures as indicated by the SIMS analysis.

References in Chapter 4

[1] J. Burm, K. Chu, W. Davis, W. J. Schaff, L. F. Eastman, T. J. Eustis, Appl. Phys. Lett. **70** (1997) 464.

[2] M. E. Lin, Z. Ma, F. Y. Huang, Z. F. Fan, L. H. Allen, H. Morkoc, Appl. Phys. Lett. **61** (1994) 1003.

[3] Z. Fan, S. N. Mohammand, W. Kim, O. Aktas, A. E. Botchkarev, H. Morkoc, Appl. Phys. Lett. **68** (1996) 1672.

[4] V. S. Fomenko, Emission Properties of Materials, Naukora Dumka, Kiev, 1981.

[5] S. Nakamura, T. Mukai, M. Senoh, Appl. Phys. Lett. **64** (1994) 1687.

[6] V. M. Bermudes, R. Kaplan, M. A. Khan, J. N. Kuznia, Phys. Rev. B **48** (1993) 2436.

[7] H. Ishikawa, S. Kobayashi, Y. Koide, S. Yamaski, S. Nagai, J. Umezaki, M. Koike, M. Murakami, J. Appl. Phys. **81** (1997) 1315.

[8] H. Ishikawa, S. Kobayashi, Y. Koide, S. Yamasaki, S. Nagai, J. Umeaaki, M. Koike, M. Murakami, J. Appl. Phys. **81** (1997) 1315.

[9] K. V. Vassilevski, M. G. Rastegaeva, A. I. Babanin, I. P. Nikitina, V. A. Dmitriev, MRS Internet J. Nitride Semicond. Res. **1** (1996) 3537

[10] T. Kim, J. Khim, S. Chae, T. Kim, Matr. Res. Soc. Symp. Proc. **468** (1997) 427

[11] D. J. King, L. Zhang, J. C. Ramer, S. D. Hersee, L. F. Lester, Mater. Res. Soc. Symp. Proc. **468** (1997) 421.

[12] L. L. Smith, R. F. Davis, M. J. Kim, R. W. Carpenter, Y. Huang, J. Mater. Res. **12** (1997) 421

[13] Y. Koide, T. Maeda, T. Kawakami, S. Fujita, T. Uemura, N. Shibata, M. Murakami, J. Electron. Mater. **28** (1999) 341

[14] J.-K, Ho, C.-S. Jong, C. C. Chiu, C.-N. Huang, C.-Y. Chen, K.-K. Shih, Appl.

Phys. Lett. **74** (1999) 1275.

[15] J. K. Kim, J.-L. Lee, J. W. Lee, H. E. Shin, Y. J. Park, T. Kim, Appl. Phys. Lett. **73** (1998) 2953.

[16] J.-L. Lee, M. Weber, J. K. Kim, J. W. Lee, Y. J. Park, T. Kim, K. Lynn, Appl. Phys. Lett **74** (1999) 2953.

[17] M. Suzuki, T. Kawakami, T. Arai, Y. Koide, T. Uemura, N. Shibata, M. Murakami, Appl. Phys. Lett. **74** (1999) 275.

[18] E. F. Scubert, W. Grieshaber, I. D. Goepfert, Appl. Phys. Lett. 69 (1996) 37371.

[19] L. Zhou, A. T. Ping, F. Khan, A. Osinsky, I. Adesida, Electron. Lett. **36** (2000) 91.

[20] Q. Z. Liu, S. S. Lau, Solid-State Electron, 42 (1998) 677.

[21] N. V. Edwards, M. D. Bremser, I. D. Goepfert, Appl. Phys. Lett. 69 (1996) 37371.

[22] V. M. Bermudez, J. Appl. Phys. **80** (1996) 1190.

[23] L. L. Smith, S. W. King, R. J. Nemanich, R. F. Davis, J. Electron. Mater. **25** (1996) 805.

[24] A. C. Schmitz, A. T. Ping, M. A. Khan, Q. Chen, J. W. Yang, and I. Adesida, Semicond. Sci. Technol., **11** (1996) 1464.

[25] Q. Z. Liu, L. S. Yu, F. Deng, S. S. Lau, J M. Redwing, J. Appl. Phys., **84** (1998) 881.

[26] Q. Z. Liu, L. S. Yu, S. S. Lau, J. M. Redwing, N. R. Perkins, and T. F. Kuech, Appl. Phys. Lett., **70** (1997) 1725.

[27] K. J. Duxstad, E. E. Haller, and K. M. Yu, J. Appl. Phys., **81** (1997) 3134.

[28] H.S. Venugopalan, S. E. Mohney, J. M. Delucca, and R. J. Molnar, Semicon. Sci. Technol. **14** (1999) 757.

[29] H. Yamagishi, Jpa. J. Appl. Phys. **23** (1984) L895.

[30] A. E. Geissberge, R. A. Sader, M. L. Balzan, and J. W. Crittes, J. Vac. Sci. Tech. **B5(6)** (1987.)

[31] E. Y. Chang, Y. L. Lai, K. C. Lin, and C. Y. Chang, J. Appl. Phys. **74** (1993) 5622.

[32] L. F. Lester, J. M. Brown, J. C. Ramer, L. Zhang, S. D. Hersee, and J. C. Jolper, Appl. Phys. Lett., **69**, 2737 (1996).

[33] G. S. Marlow and M. B. Das, Solid-State Electron. 25, 91 (1982).

[34] Z. Fan, S. N. Mohammad, W. Kim, O. Aktas, A. E. Botchkarev, and H. Morkoc, Appl. Phys. Lett. **68**, 1672 (1996).

[35] N. A. Papanicolaou, M. V. Rao, J. Jittereder, and W. T. Anderson, J. Vac. Sci. Technol. B **19**, 261 (2001).

[36] S. J. Cai, R. Li, Y. L. Chen, L. Wong, W. G. Wu, S. G. Thomas, and K. L. Wang, Electron. Lett. **34**, 2354 (1998).

[37] C. T. Lee and H. W. Kao, Appl. Phys. Lett. 76, 2364 (2000).

[38] M.Bauccio, ASM Metals Reference book, American Society for Metals, Metals Park, OH, 1994.

[39] Y. G. Shen, Y. W. Mai, Mat. Sci. Eng, **A288** (2000) 47.

[40] T. Hurkmans, T. Trinh, D.B. Lewis, J. S.Brooks and W. D. Munz, Surf and Coat Tech, **76** (1995) 159.